Clim Dyn
DOI 10.1007/s00382-010-0750-1

Influence of aerosol-radiative forcings on the diurnal and seasonal cycles of rainfall over West Africa and Eastern Atlantic Ocean using GCM simulations

Kyu-Myong Kim · William K.-M. Lau · Yogesh C. Sud · Gregory K. Walker

Received: 27 February 2009 / Accepted: 19 January 2010

Abstract Effects of aerosol radiative forcing on the diurnal and seasonal cycles of precipitation over West Africa and eastern Atlantic Ocean are investigated for the boreal summer season: June–July–August. An eight year (2000–2007) average of GCM simulated rainfall data is compared with the corresponding TRMM rainfall data. The comparison shows that the amplitude of the diurnal cycles of rainfall over land and ocean are reasonably well simulated. Over land, the phase of the simulated diurnal cycle of precipitation peaks several hours earlier than that of the TRMM data. Corresponding differences over the ocean(s) are relatively smaller. Some of the key features of the aerosol induced model simulated field anomalies are: (a) aerosol direct radiative forcing which increases the atmospheric stability and reduces the daytime moist convection and convective precipitation; (b) the aerosol induced changes in the diurnal cycle of precipitation are out of phase with those of the TRMM data over land, but are in-phase over the ocean; (c) aerosols reduce the amplitude of the diurnal cycle of precipitation over land and enhance it over ocean. However, the phase of the diurnal cycle is not affected much by the aerosol radiative forcing both over land and ocean. During the boreal summer, aerosol radiative forcing and induced circulation and precipitation cool the Sahel and the southern part of Sahara desert more than the adjacent areas to the north and south, thereby shifting the peak meridional temperature gradient northward. Consequently, an anomalous easterly jet is found north of its climatological location. This anomalous jet is associated with increased cyclonic circulation to the south of its axis, resulting in an anomalous monsoon rain belt in the Sahel.

Keywords Monsoon · Rainfall · Aerosol · Radiative forcing

1 Introduction

The primary driving force of atmospheric diurnal and seasonal cycles is the Solar insolation. In addition, the regional diurnal and seasonal variation of convective precipitation is also affected by many other factors including, but not limited to, atmospheric tides, orography, geographical location, and land-use land-cover. Numerous studies have been conducted to understand the diurnal and seasonal cycles of precipitation over land and oceans (Collier and Bowman 2004; Dai 2001; Janowiak et al. 1994; Sui et al. 1997). In general, the diurnal and seasonal variations of precipitation are larger over land as compared to oceans (Nesbitt and Zipser 2003). Over land, the convective available potential energy (CAPE) of the planetary boundary layer, which also serves as the cloud sub-layer, is directly affected by solar heating of the land surface. Therefore, the diurnal cycle of solar insolation is the primary cause of the late afternoon cumulus activity and

This paper is a contribution to the special issue on West African Climate, consisting of papers from the African Multidisciplinary Monsoon Analysis (AMMA) and West African Monsoon Modeling and Evaluation (WAMME) projects, and coordinated by Y. Xue and P. M. Ruti.

K.-M. Kim (✉)
University of Maryland Baltimore County, Baltimore, MD, USA
e-mail: kyu-myong.kim@nasa.gov

W. K.-M. Lau · Y. C. Sud
Laboratory for Atmospheres, NASA/GSFC,
Greenbelt, MD, USA

G. K. Walker
SAIC/General Sciences Operation, Beltsville, MD, USA

Published online: 13 February 2010

precipitation over land (Dai 2001). On the other hand, the diurnal cycle of surface temperature over the ocean is much weaker due to the relatively high heat capacity of the oceanic mixed-layer. Nevertheless, the atmosphere is cooled similarly over land and oceans by the outgoing longwave radiation, which in turn builds CAPE through the night. This is particularly evident over the ocean because the ocean does not cool as much as the land. Accordingly, oceanic precipitation often occurs between midnight and early morning (Randall et al. 1991).

Despite discernible progress in simulating the seasonal means and the sub-seasonal variations of precipitation, the diurnal variations of precipitation continue to be simulated poorly in almost all present-day GCMs. Compared to observations, GCMs tend to simulate too strong a diurnal cycle over land versus too weak a diurnal cycle over ocean (Collier and Bowman 2004). Moreover, many GCMs are unable to simulate the phase of the diurnal cycle of precipitation realistically. GCM Simulated land precipitation usually peaks around local noon instead of late afternoon as pointed out in many studies (Collier and Bowman 2004; Slingo et al. 2004; Dai and Trenberth 2004; Lau et al. 2007; Lee et al. 2007a). To improve the simulation of the diurnal phase of precipitation, many studies have investigated the effect of boundary-layer processes, convection triggering mechanisms (e.g., Lee et al. 2007a) and cloud base height or level (Zhang 2003).

The West African Monsoon (WAM) system is a major climate system, characterized by ITCZ-type convection, with strong oceanic control and limited poleward excursion of the monsoon rain band as compared to the Asian monsoon; the location of the WAM rainbelt is affected by heating of the Saharan desert located to the north of the WAM region (Lau et al. 2007). Consequently, seasonal variation of rainfall over West Africa occurs in concert with the seasonal migration of the ITCZ from the Gulf of Guinea to land regions of Sahel. The presence of the vast deserts to the north of the monsoon region provide strong meridional temperature gradients between the warm deserts to the north and cool equatorial monsoon regions to the south; and, together they enable an African easterly jet (AEJ) to form over the Sahel region at around 15°N (Burpee 1972; Thorncroft and Blackburn 1999). Synoptic and seasonal variation of weather and rainfall are closely related with temporal variation of AEJ (Thorncroft and Rowell 1998; Thorncroft and Blackburn 1999).

Lau et al. (2009) found that radiative heating by the elevated Saharan dust aerosols during the boreal summer influence the rainfall by heating of the upper part of the dust-layer and the atmosphere above and cooling below the dust layer of the atmosphere and the underlying surface. These heating anomalies draw in low-level moist air from the eastern Atlantic and the Gulf of Guinea into the Sahel. Over land, the incoming moist air rides over the cooler near-surface air mass thereby increasing moist convection and rainfall over the WAM land region and the eastern Atlantic ITCZ. Moreover, aerosols have the ability to interact with the solar radiation and clouds and produce considerable modulation of the diurnal temperature variation at the surface. During the daytime, aerosols scatter and/or absorb solar radiation, thereby reducing the shortwave radiation reaching the surface of the Earth. These two aerosol effects increase the stability of atmosphere below the aerosol levels. During nighttime, the longwave radiative flux emitted by dust aerosols warms the surface, and cools the upper levels, thereby promoting vertical instability. Based on these considerations, aerosol radiative effects would reduce the diurnal variation of temperature over land; however, the corresponding influences would be much smaller over ocean because of the heat capacity of the mixed layer of the ocean. In recent studies, aerosol emissions over the large industrial cities have been associated with changes in weekly and diurnal cycles of precipitation over the United States (Bell et al. 2008). Transport of aerosols and dust from desert areas is also affected by PBL stability, which has been linked to the diurnal variation of convection and atmospheric stability (Chaboureau et al. 2007). Moreover, the diurnal variation of aerosols also affects aerosol radiative forcing, as well as clouds and precipitation, by modulating the number of cloud condensation nuclei (CCN) (Kaufman et al. 2005).

During the boreal summer, June–July–August, large quantities of airborne dust aerosols uplifted from the Saharan desert and the Sahel regions by dry convection and strong winds are transported from North Africa towards the Atlantic Ocean. The hot dry air accompanying these dust outbreaks can suppress tropical cyclogenesis (Dunion and Velden 2004). Lau and Kim (2007a, b) show that Saharan dust also warms the atmosphere, whereby it affects precipitation patterns and causes widespread cooling of the tropical Atlantic ocean, all of which can impede the formation of hurricanes. At a more fundamental level, Saharan dust radiative effects impact the diurnal and seasonal cycles of precipitation over the Atlantic and West Africa (Lau et al. 2009). This motivated us to investigate the effect of aerosol radiative forcing on the diurnal cycle of precipitation over the West African monsoon region and the eastern Atlantic Ocean. In Sect. 2, model and data used in this study are described. In Sect. 3, the simulated diurnal cycle and seasonal migration of monsoon rain belt are discussed. Finally, the findings are summarized in Sect. 4.

2 Descriptions of model and experiments

We use the NASA fvGCM with NCAR physics. The fvGCM is a grid point atmospheric general circulation

model based on the finite-volume dynamical core (Lin and Rood 1996, 1997; Lin 1997). The model has 55 vertical levels and a uniform $2^{o} \times 2.5^{o}$ latitude–longitude horizontal resolution. The model was modified to use the shortwave and longwave radiative transfer scheme of Chou and Suarez (1999) and Chou et al. (2001), respectively. The precipitation schemes were replaced with a prognostic cloud scheme called Microphysics of Clouds with Relaxed Arakawa Schubert (McRAS; Sud and Walker 1999, 2003). The fvGCM is coupled to the NCAR Common Land Model (Dai et al. 2002). Daily mean SSTs are linearly interpolated from the monthly mean SSTs that are prescribed from the NCEP analysis data. For interactive SST, a simple slab ocean model is included, in which the anomalous net flux into the ocean surface is used to adjust the daily SST anomalies that are then superimposed onto the evolving SSTs as prescribed above.

The aerosol forcings are calculated from climatologically prescribed, but seasonally varying three-dimensional distributions of five species of aerosols—dust, black carbon, organic carbon, sulfate, and sea salt. The prescribed aerosol data are drawn from the Goddard Chemistry Aerosol Radiation and Transport (GOCART) model (Chin et al. 2002, 2004). The GOCART datasets have been documented and validated in several recent papers (e.g. Chin et al. 2002). Both longwave and shortwave aerosol radiative forcing are included. More details of the optical properties of aerosols and their impact on the large-scale water cycle over Atlantic Ocean and West African monsoon can be found in Lau et al. (2009).

Aerosols modify the surface fluxes of shortwave and longwave radiation. To represent their effects on the SSTs, the following simple slab ocean model (Schollaert and Merrill 1998) is used.

$$\frac{\partial T'}{\partial t} = \frac{1}{\rho C_p}\frac{\Delta F}{H} - \gamma T'$$

where T' is SST perturbation, ρ and C_p are density and heat capacity of oceanic water. The net surface heat perturbation, ΔF, calculated from the differences between daily mean simulated surface heat fluxes and the climatological mean surface net flux. H the seasonally varying mixed layer depth obtained from the global climatology from de Boyer Montegut et al. (2004), and γ a damping coefficient; a five day damping time-constant is used in this application. In this study, the atmospheric GCM and ocean slab model are coupled, while the SST is updated once every day using the daily accumulated surface net flux anomalies. Two sets of GCM simulation experiments were conducted, first without any aerosols (NA) and the second with all five species of aerosols (AA). Each simulation starts from April 1 and extends to November 1 of each of the eight years (2000–2007). However, the same aerosol distribution is prescribed in each AA simulation. All simulations are global. Only results over the West African monsoon region and Atlantic Ocean/Caribbean region are shown and discussed.

3 Results

In this study, 8-year mean diurnal cycle simulated for the boreal summer (JJA) for NA and AA model integrations are examined. For comparison, 8 years (2000–2007) of TRMM TMI data are used to define the mean diurnal cycles of precipitation over the West Africa and the eastern Atlantic Ocean. Due to the unique orbits of the TRMM satellite, the satellite visits the same place at different hours of the day, which allows TRMM data to be used for extracting the observed diurnal cycle when enough samples are available. However the number of samples depends on the latitude. In this study, we used TRMM data for eight boreal summers (JJA). In the region between 10°N and 10°S, about 45 samples for each hour are available at each grid cell. The sample numbers increase with latitude and peak at around 32°N where more than 120 samples are available for each hour. The diurnal composite for the entire period is projected onto a 24 h cycle to obtain diurnal amplitude and phase of precipitation. For the model diurnal cycle, however, data from each 24-hour period is fitted to diurnal harmonics to obtain the diurnal amplitude and phase based on hourly output. The same procedure is applied to yield the corresponding diurnal amplitude and phase of precipitation for each simulation. Statistical significance tests were conducted for the model simulated diurnal cycle following the methodology of Bell et al. (2008).

3.1 Observed and simulated precipitation diurnal cycle

Figure 1 shows the spatial distributions of the diurnal phase and amplitude of TRMM/TMI precipitation and model (NA) precipitation with respect to the local solar time. Coherent phases and amplitudes are found over the land and oceanic regions, respectively, but there are large differences between the corresponding TRMM data and model simulations. Over the ocean, the observed (TRMM) rainfall maxima occur between midnight and dawn with peaks between 3 AM and 6 AM. On the other hand, several spatially coherent patterns of the local precipitation maximum are seen over land. In the eastern US, Caribbean islands, and central South America, the precipitation tends to peak anywhere from the early afternoon to the late evening. TRMM/TMI precipitation over the Mid West/Great Plains of the continental US as well as large parts of Africa tends to peak late at night. The diurnal amplitude of precipitation is generally larger over land, except for the ITCZ over the Atlantic Ocean. Not surprisingly, very weak

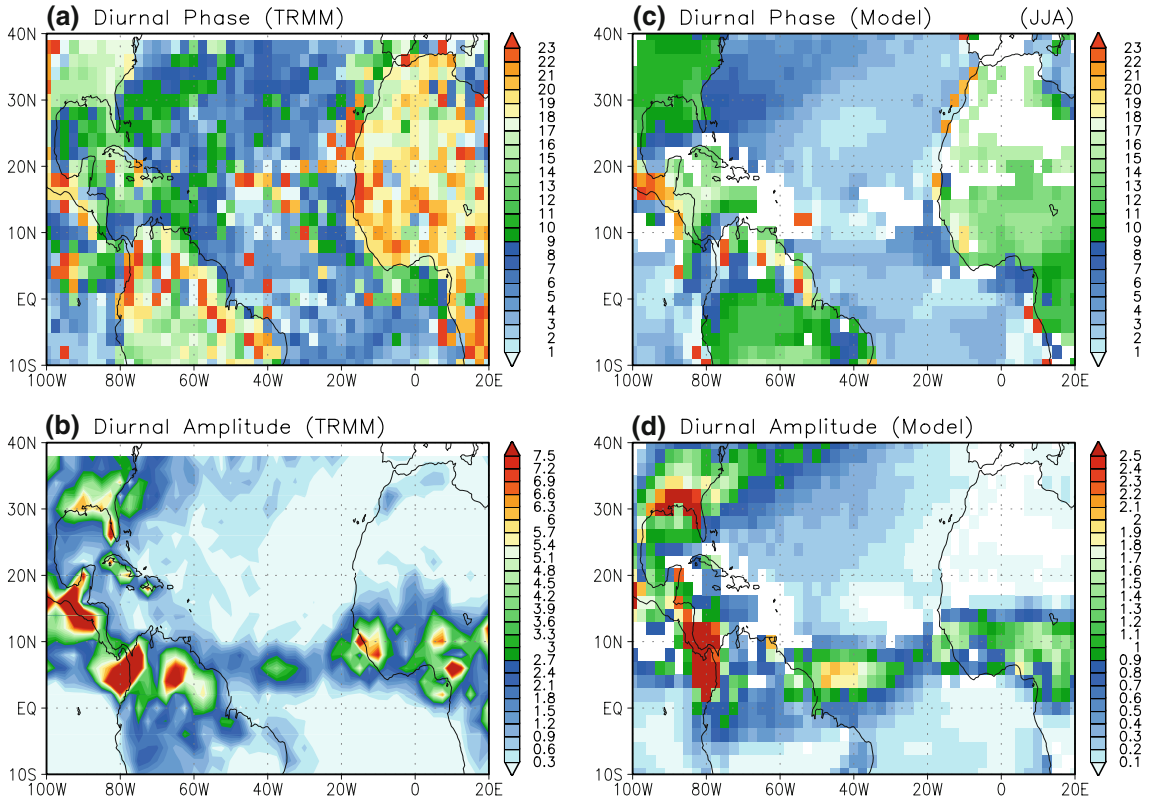

Fig. 1 Spatial distribution of **a** local solar time at the maximum and **b** the amplitude of diurnal harmonics of precipitation for June–July–August from TRMM. **c**, **d** are same as **a** and **b** except from the model. Only diurnal variability exceeding 95% statistical significance levels are shown in **c** and **d**. Units are mm/day for amplitude and local solar hour for phase

diurnal amplitudes are observed over the Sahara desert and the sub-tropical oceanic regions, where subsidence persists and the precipitation is small.

In general, the model realistically simulates the land–sea contrast of diurnal peaks. However, precipitation over land peaks in the afternoon and precipitation over ocean peaks in the early morning. Specifically, model simulated precipitation peaks between 1 and 4 AM over the ocean, which is 2–3 h sooner than that of TRMM data, which peaks around 3–6 AM. Over land, model precipitation peaks in the early afternoon in most areas; that is approximately 3 h earlier than in TRMM. Both results suggest an insufficient time delay for moisture buildup before the onset of moist convection. In the real world, deep convection follows shallow convection, slowly moistening the lower troposphere before the onset of moist convection, where as this does not happen in the model. This is a deficiency of almost all GCMs. Additionally, the model does not simulate the late night precipitation peak over the Midwest/Great Plains region of continental US and most of the northern Africa continent. Interestingly, large subtropical subsidence regions over the western North Atlantic Ocean, the southern Atlantic Ocean, and the eastern equatorial Pacific show a highly coherent pattern of diurnal precipitation that peaks between 2 AM and 3 AM. These areas happen to coincide with the stronger diurnal cycle of the model as compared to observation (Fig. 2b). Dai (2001) found a similar discrepancy in the NCAR model and related it to early morning drizzle in the dry areas. Such a discrepancy can be expected to lead to the above biases in precipitation peak over the ocean. The diurnal phase of rainfall over other parts of the ocean, especially the western Atlantic Ocean near the US shows better agreement with observations. Over land, the model simulated diurnal phase of precipitation shows a more uniform horizontal distribution especially over Africa.

Key differences in the diurnal cycle of precipitation between TRMM observation and model simulation are shown in Fig. 3. Over land, TRMM data shows broad peaks between 2 PM and 8 PM. As shown in Fig. 1, the broad peaks are due to different characteristics of land precipitation diurnal cycle between eastern US, central US, and northern Africa. Otherwise, the simulations do not show much variation in precipitation over US and Africa; both exhibit uniform peaks in the early afternoon. Previous studies suggested that the simulation of the late night peak of rainfall over the Great Plains improved with increasing resolution (Lee et al. 2007b) and/or when the convective

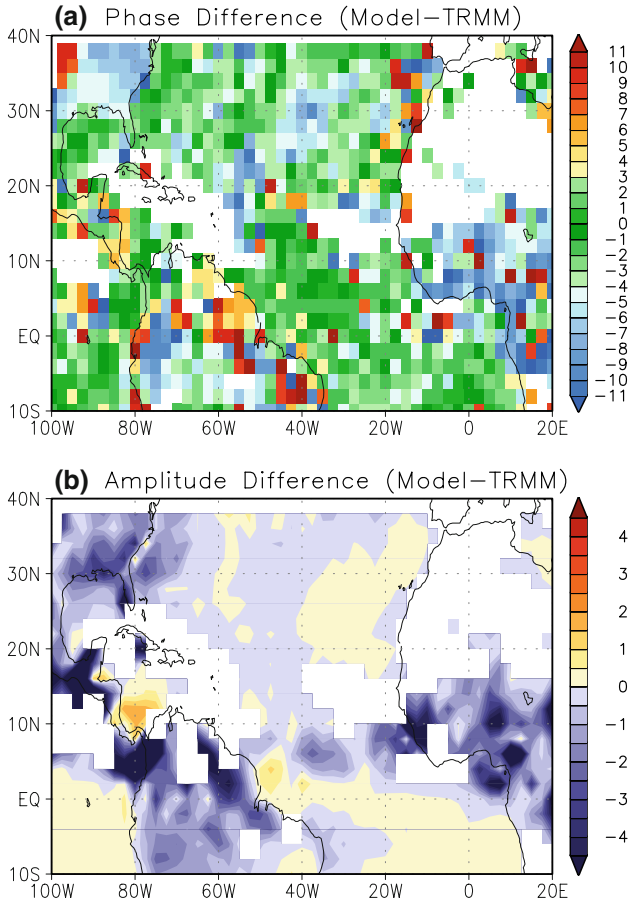

Fig. 2 Spatial distribution of **a** the local solar time at the maximum and **b** the amplitude of diurnal harmonics of precipitation difference between TRMM and model. Negative phase difference indicates the model precipitation peaks earlier than TRMM

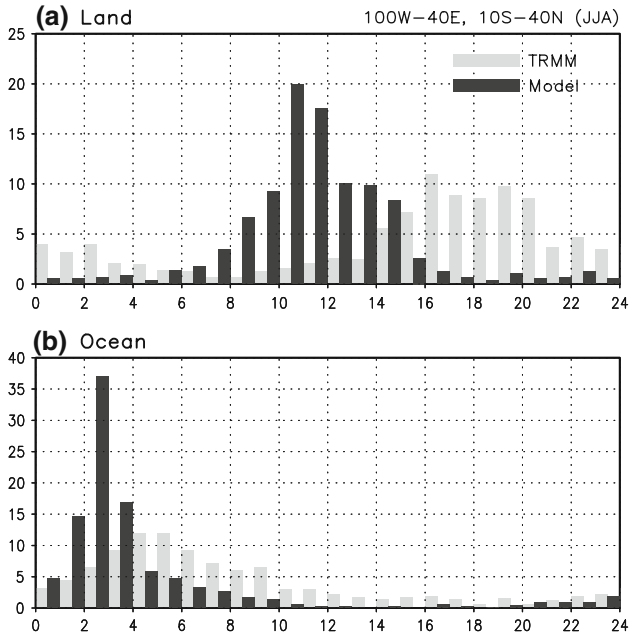

Fig. 3 Frequency (in %) distribution of local solar time at the maximum diurnal harmonics of precipitation from TRMM and model for **a** land and **b** ocean regions between 100°W–40°E and 10°S–40°N

triggers were based on the boundary layer forcing (Zhang 2003). Over land regions (of Africa), because of the longer life cycle of mesoscale convective system, the diurnal cycle of rainfall peaks in the late evening even though convective intensity peaks in the late afternoon (Nesbitt and Zipser 2003). Lack of such details, inherent in a coarse resolution model, may be the cause of poor simulations of the diurnal cycle of precipitation over the central US and Africa. Over the oceans, the phase differences between modeled and observed peaks are well within 2–3 h. The early peak in model simulated diurnal cycle of precipitation may be caused by the lack of a delayed response in convection, which is a well-known problem of most atmospheric GCMs (Lau et al. 2007; Lee et al. 2007a).

3.2 Aerosol effects on the precipitation diurnal cycle over land

To further examine the effect of aerosol radiative forcing on the diurnal cycle of precipitation, NA and AA runs are compared. All anomalies shown hereafter are difference between AA and NA runs. Figure 4 shows the diurnal amplitude differences of net surface shortwave and longwave fluxes and precipitation between AA and NA. The difference map of the diurnal amplitude of surface shortwave radiation clearly shows that the two major sources of Saharan dust, one near the northeast African continent near Algeria, and the other near the Bodele Depression (Middleton and Goudie 2001; Jeong et al. 2008), and the extension of a dusty tongue from West Africa to the Caribbean. As expected, the diurnal amplitude of the surface shortwave radiation is reduced over the area where the dust aerosols (predominantly Saharan dust) reduce the shortwave radiation reaching the surface of the Earth. In the daytime, longwave radiation differences largely mitigate the effect of shortwave radiation; thus the diurnal amplitude of longwave is reduced especially over land where the response time is short. Over the ocean the corresponding change is negligible due to the large heat capacity of the oceanic mixed layer.

With the exception of a few grid-cells, the local maxima of both land and ocean precipitation were not affected much by the aerosol radiative forcing (not shown). On the other hand, discernible changes have been simulated in the amplitude of the diurnal cycle (Fig. 4c). In general, the diurnal amplitude of precipitation over land is reduced while that over ocean is increased. The change in the amplitude over Sahel (also eastern US) is roughly 50% of the diurnal amplitude simulated by the control run (NA).

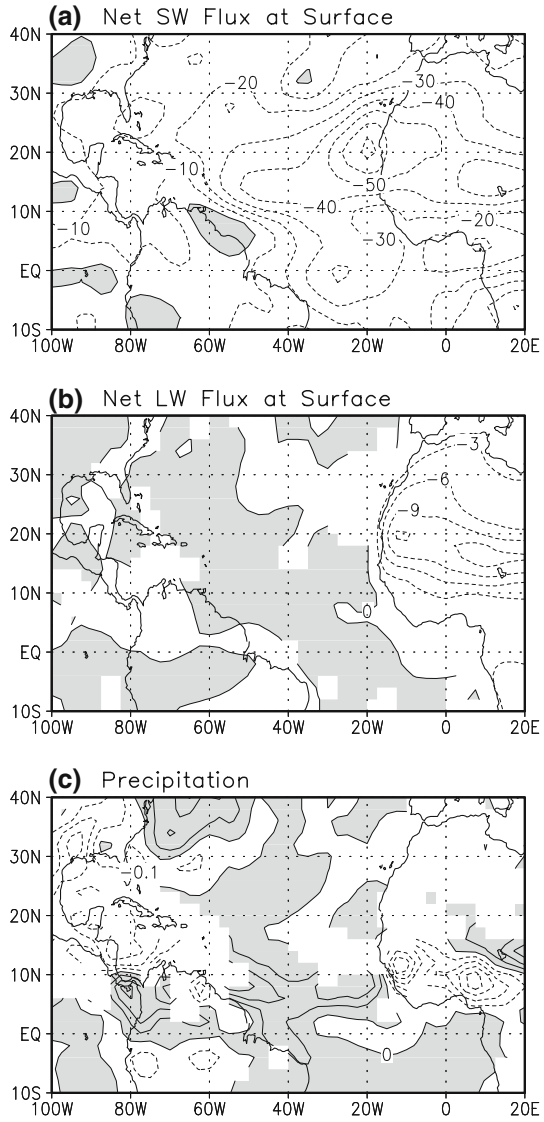

Fig. 4 Aerosol induced anomalies (AA–NA) of the diurnal amplitude of **a** surface net shortwave radiation (W m^{-2}), **b** surface net longwave radiation (W m^{-2}), and **c** total precipitation (mm day^{-1})

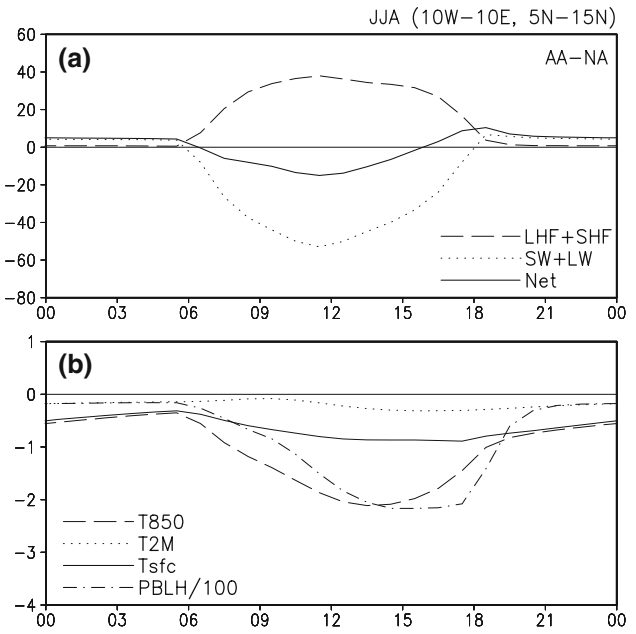

Fig. 5 Mean diurnal evolution of anomalous (AA–NA) **a** net, radiative, and heat fluxes at the surface (W m^{-2}) and **b** 850 hPa temperature (K), 2 m air temperature (K), surface temperature (K), and PBL height (m) over land (10°W–10°E, 5–15°N). PBL height is multiplied 0.01

To elucidate the reason for the different responses in the diurnal cycle of land and ocean precipitation, two subregions, one over the Sahel (5–15°N, 10°W–10°E) and the other over the eastern tropical Atlantic Ocean (35–15°W, 5–10°N) are further analyzed.

Figure 5 shows the diurnal variation of surface energy fluxes over Sahel; positive values indicate surface warming while negative values indicate surface cooling. Aerosols reduce surface net radiative flux substantially by scattering and absorbing the incoming solar irradiation. Aerosols begin to reduce surface net radiation starting at sunrise with the largest reduction ($\sim$55 W m^{-2}) at or around local noontime. Outgoing longwave flux is also reduced, partly because the cooler surface emits less, and partly because the downward longwave flux increases from the warmer aerosol layer containing dust. The reduced net upward longwave flux at the surface is not large enough to compensate for the increase in shortwave cooling during the day, but the surface starts to get warmer near sunset due to the reduction of longwave fluxes (Fig. 5a).

A large part of the reduction of surface net radiative flux (caused by aerosol radiative forcing) is compensated by decreased surface latent and sensible heat fluxes. The net heat flux (shown as solid line on Fig. 5a) indicates that aerosols cool the surface during the day and warm it at night.

Both scattering and absorption by aerosols reduce the shortwave flux reaching the surface, but absorbing aerosols, such as dust, warm the lower to mid troposphere where the aerosols are. Accordingly, aerosols cool the surface more than the atmosphere, and hence increase atmospheric stability and lower the planetary boundary layer height (Fig. 5b). The diurnal temperature range can be expected to either increase or decrease, depending on the optical properties of aerosols, as in Yu et al. (2002), who also found that scattering aerosols decrease the diurnal temperature range, but absorbing aerosols can increase the temperature range. However, in our simulations most of the absorbing aerosols are lofted with the Saharan air layer, thus the diurnal cycle of the surface air temperature weakens as shown in Fig. 5b. Stronger daytime cooling, which decreases with height, leads to a more stable atmosphere and a shallow boundary-layer. The anomalous temperature difference between the surface and 850 hPa is

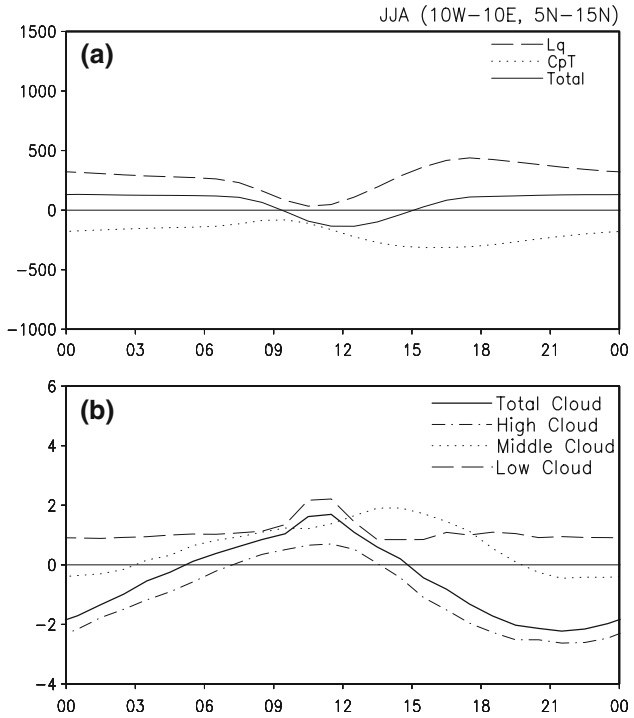

Fig. 6 Same as Fig. 5, except for **a** latent, internal and total specific energy and **b** cloud amount at different layers. Units are J kg^{-1} for **a** and % for **b**

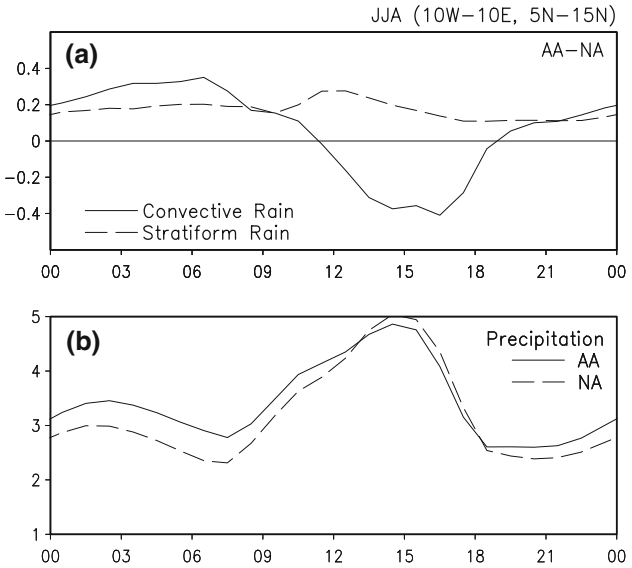

Fig. 7 Mean diurnal evolution of **a** convective and stratiform precipitation difference between AA and NA runs, and **b** seasonal mean precipitation from AA and NA runs, over land (10°W– 10°E, 5–15°N). Units are mm day^{-1}

larger during the day as opposed to the night. The time of the maximum cooling at the surface is around 4 PM when the net surface heat flux flips sign (Fig. 5a). On the other hand, the maximum cooling at 850 hPa occurs several hours after the maximum cooling at the surface.

Figure 6a shows the diurnal cycle of temperature and moisture at 850 hPa. To understand these changes, the results are shown in the form of latent energy (L_q), sensible energy (C_pT), and total specific energy content of air ($L_q + C_pT + gh + (u2 + v2)/2$). As also shown in Fig. 5b, the anomalous diurnal cycle of temperature at 850 hPa peaks in the early morning and continues to decrease with sunrise due to aerosol effects. However, the latent energy (L_q) at 850 hPa increases over the day due to aerosol radiative forcing. Since the surface latent heat flux decreases with aerosol radiative forcing (Fig. 5a), the moisture increase at 850 hPa is consistent with increased moisture convergence (not shown) initiated by shortwave heating by dust and intensified by seasonal monsoon flow (Lau et al. 2009). Minimum moisture between 9 LST and 15 LST is also consistent with a decrease in net surface heat flux (Fig. 5a) and an increase of cloud cover (Fig. 6b). The diurnal variation of total moist static energy suggests that the lower troposphere becomes anomalously unstable during nighttime. The diurnal variation of clouds shown in Fig. 6b is consistent with the diurnal cycle of moist static energy. The temporal variation of total cloud cover is largely related to high clouds. Because of the stabilizing effect of the aerosol radiative forcing, high cloud cover is reduced on most days except for the brief increase between early mornings to afternoon. However, mid- to low-cloud cover increases over the day because any clouds emerging due to the instability at the sub-cloud layer are capped by the larger stability aloft, i.e., between low to mid level (Fig. 6b).

While the lower troposphere is stabilized by the aerosol effect, which varies as a function of height, increased moisture and nocturnal cooling destabilize the lower atmosphere during the nighttime. As a result, convective precipitation is reduced during the daytime by $\sim$10%, while nighttime, between 11 PM and 7 AM, convective rain is increased more than 10%, with a maximum increase of 30% occurring between 6 AM and 7 AM (Fig. 7a). However, because of an increase in the moisture convergence in the lower troposphere, the low-level moisture and stratiform rain is increased both in the daytime and nighttime. As a result, precipitation in the evening to early morning hours increases in aerosol runs, while early afternoon precipitation decreases due to the stabilizing effects of the aerosol (Fig. 7b). The aerosol induced change in the diurnal cycle of precipitation on land is out-of-phase with the diurnal cycle in NA runs. Overall, aerosols reduce the amplitude of the diurnal variation of precipitation over land.

3.3 Aerosol effects on the precipitation diurnal cycle over ocean

As compared to land, the diurnal variations of low-level temperature and moisture are relatively weak. Figure 8a

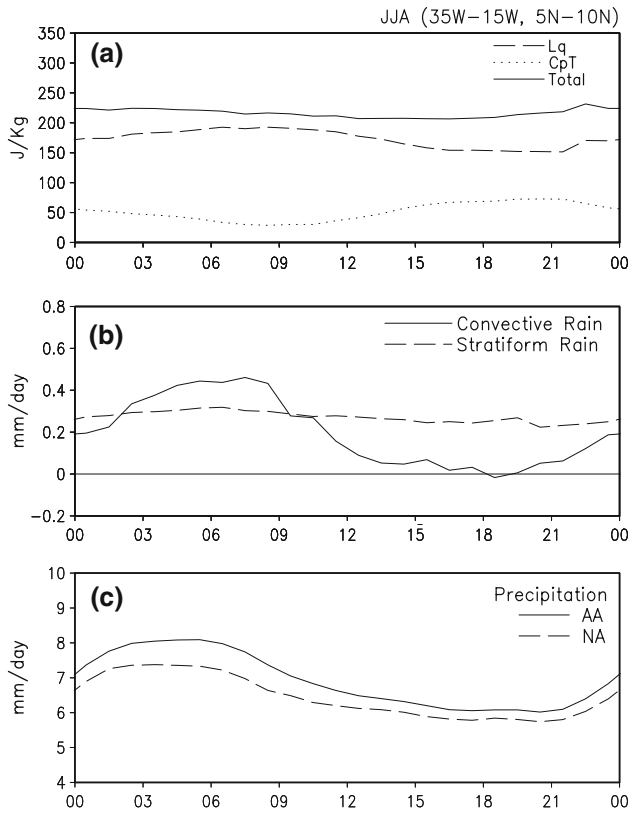

Fig. 8 Mean diurnal evolution of **a** latent, internal, and total specific energy, **b** convective and stratiform precipitation difference between AA and NA runs, and **c** precipitation from AA and NA run over ocean (35–15°W, 5–10°N). Units are J kg^{-1} for **a** and mm day^{-1} for **b** and **c**

shows the diurnal cycle of latent (L_q) and sensible (C_pT) energies at 850 hPa over the eastern Atlantic Ocean (35–15°W, 5–10°N). The time of the peak of the latent energy is in-phase with the diurnal variation of boundary-layer height and vertical velocity at 850 hPa (not shown) and out-of-phase with that of the internal energy (Fig. 8a). This result indicates that during the early morning peak of diurnal precipitation, surface-layer instability grows with downdraft cooling (Sud et al. 1999) and thus both evaporation (shown) and sensible heat fluxes increase (not shown). This is closely linked to the presence of convective precipitation (Fig. 8b). The aerosol induced change in the diurnal cycle of precipitation is in-phase with the simulated diurnal cycle of precipitation over the ocean. Thus aerosols increase the amplitude of diurnal variation of precipitation over the ocean (Fig. 8c). However, the large-scale precipitation is increased throughout the day, which is consistent with moisture convergence induced or caused by the dust radiative forcing over Sahel and eastern Atlantic Ocean (Lau et al. 2009).

The above results are consistent with the characteristics of rainfall diurnal variation under radiative–convective feedback mechanisms (Randall et al. 1991). Due to the high heat capacity of water, solar insolation does not warm the ocean surface as much as land surface. On the other hand, shortwave heating of the atmosphere evaporates the cloud water and inhibits the development of convection. At night, longwave cooling at the top of clouds increases atmospheric instability and the development of moist convection, which peaks in the early morning. In the presence of aerosols, the shortwave reduction at the ocean surface will increase atmospheric stability while the shortwave absorption by dust will increase atmospheric temperature, which further increases atmospheric stability and promotes the evaporation of existing cloud water. At night, dust longwave radiative forcing is positive at the surface and negative in the atmosphere. The net effect is to increase longwave radiative cooling of the atmosphere and warming of the surface, both of which increase the atmospheric instability.

In this study, the atmosphere and ocean are coupled with once a day SST updates. In the real world, however, the SST response to aerosol radiative forcing will also have a diurnal variation which is ignored in this study. Shortwave reduction occurs during daytime, while only longwave emission by dust (that occurs all the time) warms the surface at night. As a result, SST anomalies due to dust radiative forcing are positive at night and negative during the day. Therefore, the diurnal cycle of precipitation change simulated by the model may slightly underestimate the aerosol influence due to the lack of ocean–atmosphere coupling on shorter time scales.

3.4 Aerosol effects on the seasonal migration of the rain belt

In this section, the effect of aerosols, especially the Saharan dust radiative forcing on the monsoon precipitation over West African monsoon is discussed.

Figure 9 shows the latitude–time cross sections of climatological mean precipitation of the control simulation (NA) together with the precipitation difference between AA (all aerosol simulation) and NA over the West African monsoon region (Fig. 9a, b) and over the eastern Atlantic Ocean (Fig. 9c, d). During the pre-monsoon season, the rain belt stays over the Gulf of Guinea (Fig. 9a). Beginning late May, the rain belt starts to migrate northward and advances into the land region of West Africa. By mid-July, the rain belt reaches 10°N and remains there until mid-August, after which time the rain belt starts to retreat southward. The seasonal migration of the center of the rain belt is well simulated by the model; however, the meridional extent of the rain belt is narrower compared to the observations as shown in Lau et al. (2007). For example, for August, the 1 mm/day contour of simulated rain rate (Fig. 9a) is located around 15°N while the observed

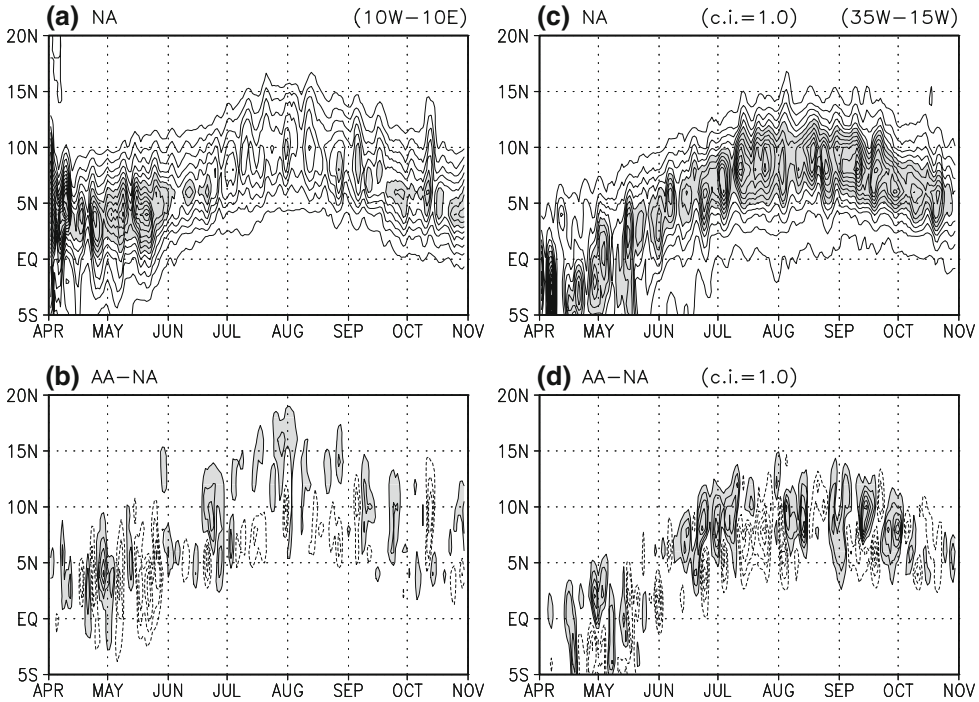

Fig. 9 Time latitude cross-section of **a** daily climatology of precipitation from NA run and **b** difference between AA and NA runs for land region (10°W–10°E). **c**, **d** are same as in **a** and **b** except for ocean region (35–15°W). Contour interval is 1.0 mm day^{-1} and zero lines are omitted

contour extends as far as 20°N. The maximum rainfall center in July and August is located at 10°N and the maximum rain rate is about 5–6 mm/day. Observations based on the merged satellite data products from GPCP shows the center of rain belt over land is located a little further north (at ~11°N) and the maximum rain rate reaches ~9 mm/day (not shown). The model reasonably simulates the center location and intensity of the rain belt during monsoon retreat in September and October. Over the ocean, the location of the rain belt is well simulated in June–July–August, but the rain rate at the center of the rain belt is less than the observed (Fig. 9c). In general, the rain belt over ocean is narrower compared to the observations, especially in September and October when the rain belt extends further north.

As shown in Fig. 9b aerosols enhance precipitation over the northern part of the rain belt, especially for the June through September periods. The present results are consistent with Lau et al. (2009), which show that the enhanced precipitation is induced by the elevated heating by Saharan dust in conjunction with the formation of a direct circulation cell with rising motion over the Sahel region, and sinking motion over the Gulf of New Guinea. Given the model bias in the northward extent of the rain belt, the increase in rainfall over the northern part of the rain belt is an improvement in the precipitation simulation attributable to the direct effect of aerosols in AA (also see Xue et al. 2009). Over the ocean, the ITCZ rain belt shows smooth northward migration, i.e., from the equator in boreal spring to 8°N in mid-July (Fig. 9c). Aerosols also increased the precipitation in the northern part of the rain belt (Fig. 9d) and this increase is also found over land.

To explore the possible mechanisms for the northward shift of rain belts over the ocean and land, the easterly jet and associated wave activities are investigated. The easterly jet over West Africa is largely a response to the thermal gradients caused by the warm desert to the north of Sahel and the cool land and ocean to the south. Figure 10b shows simulated differences of vertically integrated meridional temperature gradient from 1,000 to 600 hPa between AA and NA. The pattern of the meridional temperature gradient difference (Fig. 10a) is consistent with the pattern of surface net radiative cooling by dust (Fig. 4a). In NA runs, the maximum temperature gradient is located to the south of the Saharan desert. In AA runs, the surface temperature over Saharan desert is much cooler than that of NA runs. Accordingly, the positive center of the meridional temperature gradient is moved further north (from 10 to 20°N) from its climatological location in AA runs, as is the easterly jet (Fig. 10c). As a result, aerosols strengthen (weaken) the easterly jet northward (southward) of the axis of the jet. The zonal wind anomalies at 600 hPa (Fig. 10c) imply an increase in cyclonic vorticity south of 20°N and a decrease in anti-cyclonic vorticity north of 20°N. To reconfirm the above explanation, the aerosol induced change of the easterly wave activities is examined. In this study, easterly wave activities are defined as a standard deviation of the filtered (6–9 days and/or 3–5 days) time-series of meridional wind at 700 hPa for June–July–August–September. Figure 10d shows that the

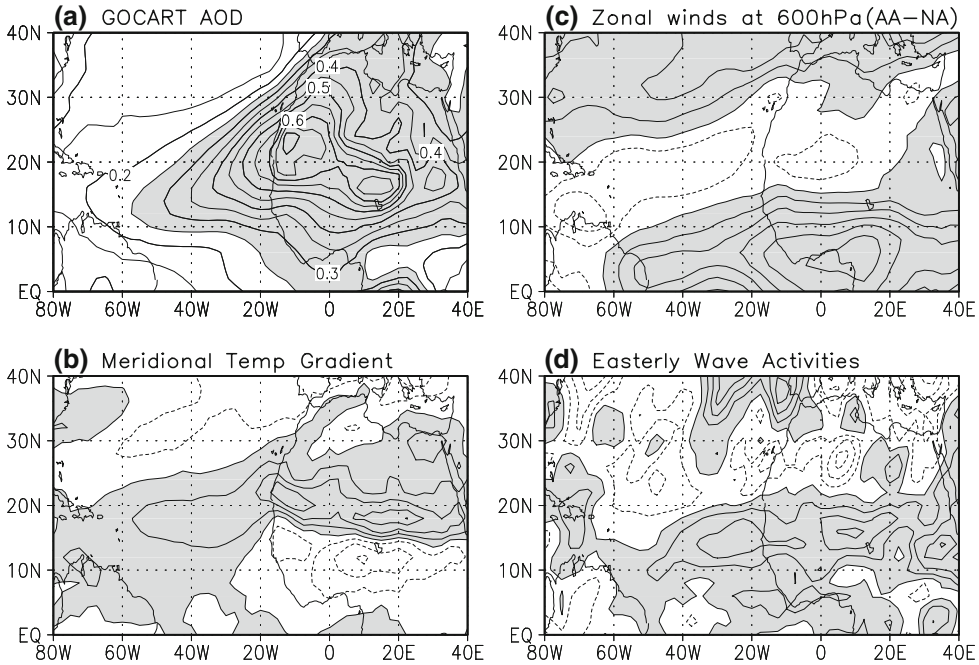

Fig. 10 Spatial distribution of **a** JJA mean GOCART aerosol optical depth (unitless), **b** meridional temperature gradient (K per 1 latitude), **c** zonal wind at 600 hPa (m s^{-1}), and **d** easterly wave activity (m s^{-1}) difference between AA and NA runs

6–9 day wave activities increase to the south and decrease to the north of easterly jet ($\sim$20°N). On the other hand, the 3–5 day wave activities increase uniformly over West Africa and the eastern Atlantic Ocean except for over the north-west coast of Africa (not shown). These results are consistent with those of Diedhiou et al. (1999) who show that the 3–5 day waves are associated with meridionally extended rainfall anomalies and the 6–9 day waves are linked to a zonally extended meridional dipole pattern of rainfall anomalies, with anti-cyclonic (cyclonic) circulation to the north (south) of enhanced easterly jet.

4 Summary and conclusion

The effects of aerosol direct radiative forcing on the diurnal cycle of precipitation over West Africa and the eastern Atlantic Ocean have been investigated with an atmospheric general circulation model coupled to a simple slab ocean model for providing the aerosol induced SST anomalies. Two sets of simulation experiments, one with and one without aerosol radiative forcing, were performed. Each set has eight ensembles with initial conditions for 1 April of years: 2000–2007. An identical aerosol distribution is prescribed in all eight simulations.

Some model biases/characteristics are identified in the analysis as follows. It simulates stronger (weaker) than the observed diurnal cycle of precipitation over land (oceans) regardless of the direct effect of aerosols. The phase of the diurnal cycle of precipitation peaks several hours earlier than that of the TRMM data. Over land, TRMM data show the broad peaks between 2 PM and 8 PM; exhibiting large variations over eastern US, central US, and northern Africa. On the other hand, the model simulates uniform peaks mostly in the early afternoon over the above domains. Over the ocean, the modeled precipitation peaks are 2–3 h earlier than the TRMM observations.

Regardless of the above, our results are useful as well as consistent with other modeling simulation results. First, both scattering and absorption reduce shortwave radiation reaching the surface while absorption by aerosols warms the lower to mid troposphere where the aerosols are found. Consequently, aerosols cool the Earth's surface and warm the atmosphere, thereby increasing the atmospheric stability and reducing the daytime moist-convection and precipitation. The shortwave absorption by aerosols enhances convection in a moist and warm environment, as is typical during the pre-mosoon season (Lau et al. 2006). When such aerosol forced warming leads to rising motion (because of nearly dry lapse rate over the desert), the near surface horizontal moisture convergence becomes stronger, producing stratiform clouds and precipitation. Thus, increased moisture and clouds at or just above aerosol levels can produce enhanced nocturnal cooling and increase the saturation moist static instability, which in turn affects moist convection. The anomalous diurnal cycle is out-of-phase (in-phase) with the typical precipitation diurnal cycle over land (ocean). In this way, aerosols reduce (increase) the amplitude of the diurnal cycle of precipitation over land (ocean). However, the phase of the

diurnal cycle is not affected much by the aerosol radiative forcing in these simulations.

The seasonal north–south migration of the center of the rain belt is well simulated by the model. However, as compared to TRMM observations reported in Lau et al. (2007), the meridional extent of the rain belt is too narrow and stays to the south of 15°N. Aerosol radiative forcing over the African continent modulates the meridional temperature gradient in such a way that the easterly jet shifts northward, increasing cyclonic circulation to the south of the jet-axis, i.e., over Sahel, thereby enhancing the precipitation, and easterly wave activity in the northward portion of the rain belt.

As a final remark, we would like to project that the diurnal cycle of precipitation will be further modulated if the aerosol indirect effects were to be invoked. Here, we merely point out that proper parameterization of aerosol–cloud radiation interactions through the direct and indirect effects has the potential to yield better simulations of the diurnal cycle of precipitation. Consequently, it will be a subject of more extensive studies with the new upcoming model that includes a parameterization of the indirect effect of aerosols.

Acknowledgments This work is supported jointly by the Precipitation Measuring Mission, the NASA AMMA program, and the program on Interdisciplinary Investigation, NASA Headquarters, Earth Science Division. Resources supporting this work were provided by the NASA High-End Computing (HEC) Program through the NASA Center for Computational Sciences (NCCS) at Goddard Space Flight Center. The authors are grateful to Dr. Eric Wilcox and two anonymous reviewers for their constructive comments. The first author wishes to thank Dr. Myong-In Lee for useful discussions.

References

Bell TL, Rosenfeld D, Kim KM, Yoo JM, Lee MI, Hahnenberger M (2008) Midweek increase in U.S. summer rain and storm heights suggests air pollution invigorates rainstorms. J Geophys Res 113:D02209. doi:10.1029/2007JD008623

Burpee RW (1972) The origin and structure of easterly waves in the lower troposphere of North Africa. J Atmos Sci 29:77–90

Chaboureau JP, Tulet P, Mari C (2007) Diurnal cycle of dust and cirrus over West Africa as seen from Meteosat Second Generation satellite and a regional forecast model. Geophys Res Lett 34:L02822. doi:10.1029/2006GL027771

Chin M, Ginoux P, Kinne S, Torres O, Holben BN, Duncan BN, Martin RV, Logan JA, Higurashi A, Nakajima T (2002) Tropospheric aerosol optical thickness from the GOCART model and comparisons with satellite and sun photometer measurements. J Atmos Sci 59:461–483

Chin M, Chu DA, Levy R, Remer L, Kaufman Y, Holben BN, Eck T, Ginoux P, Gao Q (2004) Aerosol distribution in the Northern Hemisphere during ACE-Asia: results from global model, satellite observations, and Sun photometer measurements. J Geophys Res 109 (D23). doi:10.1029/2004GL02014

Chou MD, Suarez MJ (1999) A solar radiation parameterization for atmospheric studies, NASA NASA Tech. Memo. 104606, vol 15, 38 pp

Chou MD, Suarez MJ, Liang XJ, Yan MMH (2001) A thermal infrared radiation parameterization for atmospheric studies. NASA Tech. Memo. 104606, vol 19, 102 pp

Collier JC, Bowman KP (2004) Diurnal cycle of tropical precipitation in a general circulation model. J Geophys Res 109:D17105. doi:10.1029/2004JD004818

Dai A (2001) Global precipitation and thunderstorm frequencies, Part II: diurnal variations. J Clim 14:1112–1128

Dai A, Trenberth KE (2004) The diurnal cycle and its depiction in the Community Climate System Model. J Clim 17:930–951

Dai Y, Zeng X, Dickinson RE, Baker I, Bonan G, Bosilovich M, Denning S, Dirmeyer P, Houser P, Niu G, Oleson K, Schlosser A, Yang ZL (2002) The common land model (CLM). Bull Am Meteorol Soc 84:1013–1023

de Boyer Montegut C, Madec G, Fischer AS, Lazar A, Iudicone D (2004) Mixed layer depth over the global ocean: an examination of profile data and a profile-based climatology. J Geophys Res 109. doi:10.1029/2004JC002378

Diedhiou A, Janicot S, Viltard A, de Felice P, Laurent H (1999) Easterly wave regimes and associated convection over West Africa and tropical Atlantic: results from the NCEP/NCAR and ECMWF reanalyses. Clim Dyn 15:795–822

Dunion JP, Velden CS (2004) The impact of the Saharan air layer on Atlantic tropical cyclone activity. Bull Am Meteorol Soc 85:353–365

Janowiak JE, Arkin PA, Morrissey M (1994) An examination of the diurnal cycle in oceanic tropical precipitation using satellite and in situ data. Mon Weather Rev 122:2296–2311

Jeong MJ, Tsay SC, Ji Q, Hsu NC, Hansell RA, Lee J (2008) Ground-based measurements of airborne Saharan dust in marine environment during the NAMMA field experiment. Geophys Res Lett 35:L20805. doi:10.1029/2008GL035587

Kaufman YJ, Koren I, Remer LA, Rosenfeld D, Rudich Y (2005) The effect of smoke, dust and pollution aerosol on shallow cloud development over the Atlantic Ocean. Proc Natl Acad Sci 102(32):11207–11212

Lau KM, Kim KM (2007a) How nature foiled the 2006 hurricane forecasts. Eos Trans AGU 88(9):105–107

Lau KM, Kim KM (2007b) Cooling of the Atlantic by Saharan dust. Geophys Res Lett 34:L23811. doi:10.1029/2007GL031538

Lau KM, Kim MK, Kim KM (2006) Asian monsoon anomalies induced by aerosol direct effects: the role of the Tibetan Plateau. Clim Dyn. doi:10.1007/s00382-006-0114-z

Lau KM, Kim KM, Lee MI (2007) Characteristics of diurnal and seasonal cycles in global monsoon systems. J Meteorol Soc Jpn 85A:403–416

Lau KM, Kim KM, Sud YC, Walker GK (2009) A GCM study of the response of the atmospheric water cycle of West Africa and the Atlantic to Saharan dust radiative forcing. Geophys Ann 27:4023–4037

Lee MI, Schubert SD, Suarez MJ, Bell TL, Kim KM (2007a) Diurnal cycle of precipitation in the NASA Seasonal to Interannual Prediction Project atmospheric general circulation model. J Geophys Res 112:D16111. doi:10.1029/2006JD008346

Lee MI, Schubert SD, Suarez MJ, Held IM, Kumar A, Bell TL, Schemm JKE, Lau NC, Ploshay JJ, Kim HK, Yoo SH (2007b) Sensitivity to horizontal resolution in the AGCM simulations of warm season diurnal cycle of precipitation over the United States and northern Mexico. J Clim 20:1862–1881

Lin SJ (1997) A finite-volume integration method for computing pressure gradient forces in general vertical coordinates. Q J R Meteorol Soc 123:1749–1762

Lin SJ, Rood RB (1996) Multidimensional flux form semi-Lagrangian transport scheme. Mon Weather Rev 124:2046–2070

Lin SJ, Rood RB (1997) An explicit flux-form semi-Lagrangian shallow water model on the sphere. Q J R Meteorol Soc 123:2477–2498

Middleton NJ, Goudie AS (2001) Saharan dust: sources and trajectories. Trans Inst Br Geogr 26:165–181

Nesbitt SW, Zipser EJ (2003) The diurnal cycle of rainfall and convective intensity according to three years of TRMM measurements. J Clim 16:1456–1475

Randall DA, Harshvardhan, Dazlich DA (1991) Diurnal variability of the hydrological cycle in a general circulation model. J Atmos Sci 48:40–62

Schollaert SE, Merrill JT (1998) Cooler sea surface west of the Sahara Desert correlated to dust events. Geophys Res Lett 25(18):3529–3532. doi:10.1029/98GL52591

Slingo A, Hodges KI, Robinson GJ (2004) Simulation of the diurnal cycle in a climate model and its evaluation using data from Meteosat 7. Q J R Meteorol Soc 130:1449–1467

Sud YC, Walker GK (1999) Microphysics of clouds with relaxed Arakawa-Schubert Scheme (McRAS). Part II: implementation and performance in GEOS 2 GCM. J Atmos Sci 56:3121–3240

Sud YC, Walker GK (2003) Influence of ice-phase physics of hydrometeors on moist convection. Geophys Res Lett 30(14):1758. doi:10.1029/2003GL017587

Sud YC, Walker GK, Lau KM (1999) Mechanisms regulating deep moist convection and sea-surface temperature in the tropics. Geophys Res Lett 26(8):1019–1022

Sui CH, Lau KM, Takayabu YN, Short DA (1997) Diurnal variations in tropical oceanic cumulus convection during TOGA COARE. J Atmos Sci 54:639–655

Thorncroft CD, Blackburn M (1999) Maintenance of the African easterly jet. Q J R Meterol Soc 125:763–786

Thorncroft CD, Rowell DP (1998) Interannual variability of African wave activity in a general circulation model. Int J Climatol 18:1305–1323

Xue Y, De Sales F, Lau WKM, Boone A, Feng J, Dirmeyer P, Guo Z, Kim KM, Kitoh A, Kumar V, Poccard-Leclercq I, Mahowald N, Moufouma-Okia W, Pegion P, Rowell DP, Schemm J, Schubert SD, Sealy A, Thiaw WM, Vintzileos A, Williams SF, Wu MLC (2009) Intercomparison and analyses of the West African Monsoon and its variability in the West African Monsoon Modeling and Evaluation Project (WAMME): First Model Intercomparison Experiment. Clim Dyn (submitted)

Yu H, Liu SC, Dickinson RE (2002) Radiative effects of aerosols on the evolution of the atmospheric boundary layer. J Geophys Res 107(D12):4142. doi:10.1029/2001JD000754

Zhang GJ (2003) Roles of tropospheric and boundary layer forcing in the diurnal cycle of convection in the U.S. southern great plains. Geophys Res Lett 24:2281. doi:10.1029/2003GL018554